View metadata, citation and similar papers at core.ac.uk
brought to you by CORE
provided by Leiden University Scholarly Publications

ASTRONOMY AND ASTROPHYSICS

Weak ice absorption features at 7.24 and 7.41 μm in the spectrum of the obscured young stellar object W 33A*

W.A. Schutte[1], A.C.A. Boogert[2], A.G.G.M. Tielens[2], D.C.B. Whittet[3], P.A. Gerakines[3], J.E. Chiar[4], P. Ehrenfreund[1], J.M. Greenberg[1], E.F. van Dishoeck[1], and Th. de Graauw[5]

[1] Raymond and Beverly Sackler Observatory Laboratory at Leiden University, P.O. Box 9513, 2300 RA, Leiden, The Netherlands (schutte@strw.leidenuniv.nl)
[2] Kapteyn Astronomical Institute, P.O. Box 800, 9700 AV, Groningen, The Netherlands
[3] Department of Physics, Applied Physics and Astronomy, Rensselaer Polytechnic Institute, Troy, NY 12180, USA
[4] NASA-Ames Research Center, MS 245-3, Moffett Field, CA 94035, USA
[5] SRON, P.O. Box 800, 9700 AV, Groningen, The Netherlands

Received 27 August 1998 / Accepted 10 December 1998

Abstract. ISO-SWS observations of the highly obscured young stellar object W 33A reveal two broad absorption features centered at 7.24 and 7.41 μm. Comparison to interstellar ice analogs shows that the 7.24 μm band can be well matched by the CH deformation mode of formic acid (HCOOH), while the 7.41 μm band can be fitted both by the formate ion ($HCOO^-$) and acetaldehyde (CH_3HCO). The laboratory spectra reveal additional strong features of these molecules which should make a more definite identification straightforward. While an assignment of the 7.24 μm band to the $-CH_3$ deformation mode of aliphatic species may be considered, the absence of a corresponding strong CH stretching mode argues against this possibility. These results and the earlier tentative detection of HCOOH towards NGC7538:IRS9 suggest that formic acid is a general component of the ices in the vicinity of embedded high-mass young stellar objects.

Key words: infrared: ISM: lines and bands – ISM: molecules – ISM: abundances – stars: individual: NGC 7538:IRS 9 – stars: individual: W 33A – methods: laboratory

1. Introduction

Icy grain mantles are an important constituent of protostellar regions. Their composition reflects the chemical conditions in the gas phase at the time of accretion. Additionally, upon release into the gas phase during the star formation process, the molecules which were stored in the mantles dominate the chemical evolution of the protostellar cloud (Charnley et al. 1992; Caselli et al. 1993). Thus, to understand the chemistry of protostellar regions, it is vital to study the composition of the icy grain mantles.

The composition of the grain mantles can be deduced from the absorption features caused by vibrational transitions of ice components in the mid-infrared (2.5–25 μm) spectra of protostellar sources. Such data are interpreted by comparison with the spectra of astrophysical ice analogs obtained under simulated space conditions. With the launch of the Infrared Space Observatory (ISO; Kessler et al. 1996) carrying the Short Wavelength Spectrometer (SWS; de Graauw et al. 1996a), for the first time it has become possible to observe the entire mid-infrared spectrum at high resolution. These new data together with earlier ground-based spectra show that the ice mantles are dominated by H_2O, with considerable quantities of CO_2, CO, CH_3OH, CH_4, and "XCN" (Whittet et al. 1996).

Its exceptionally high ice column density and considerable brightness in the mid-infrared (3.4–8 μm) has traditionally made the high-mass embedded young stellar object (YSO) W 33A (R.A.(2000)=18h14m39.0s; Decl.(2000)=-17°52′04″) the object of choice when searching ice components of moderate and low abundance. Solid CO, "XCN", CH_3OH, OCS and CH_4 were all first detected here (Lacy et al. 1984, 1991; Grim et al. 1991; Geballe et al. 1985; Palumbo et al. 1995). This paper presents the full 7–8 μm spectrum of W 33A obtained by the ISO-SWS. Prior to ISO, only low resolution Kuiper Airborne Observatory and high resolution ground-based data were available in the 7–8 μm region (Tielens 1989; Lacy et al. 1991; Boogert et al. 1997), but all were severely plagued by telluric absorption. Thus ISO allows the first good look in this spectral region.

The 7–8 μm region is very promising for probing absorption bands of solid state molecules. Earlier the detection of the CH_4 ν_4 feature at 7.67 μm and, tentatively, the SO_2 ν_3 feature at 7.6 μm towards W 33A were reported (Boogert et al. 1996; 1997; 1998). However, the important 7.0–7.5 μm region, encompassing, a.o., the CH deformation modes of small organic molecules, has not been previously studied. A preliminary account of this work was published earlier (Schutte et al. 1998a).

Send offprint requests to: W.A. Schutte (schutte@strw.leidenuniv.nl)

* Based on observations with ISO, an ESA project with instruments funded by ESA Member States (especially the PI countries: France, Germany, the Netherlands and the United Kingdom) and with the participation of ISAS and NASA.

We note that the important 5–7 μm region of W 33A will be shown and discussed in a future paper (Keane et al., in preparation).

The layout of this paper is as follows. In Sect. 2 we briefly summarize the known characteristics of W 33A. Sect. 3 reviews the observational aspects and presents the new ISO-SWS data. Sect. 4 compares the detected absorption features at 7.24 and 7.41 μm with absorption features of dust in the diffuse medium to investigate the possibility of an origin in the refractory grain component (silicates, carbonaceous matter). Sect. 5 briefly discusses the particulars of the experimental production of the astrophysical ice analogs used for comparison to the new data. In Sect. 6, the W 33A spectrum is compared to spectroscopy of a number of molecules embedded in astrophysical ice analogs. Sect. 7 predicts how additional infrared features of the candidate species could show up in future ISO spectra. Sect. 8 then discusses the implications of our results for the chemical evolution of ices near massive YSO's. Sect. 9, finally, summarizes the conclusions of this study.

2. The object

W 33A is a highly luminous young stellar object (L $\approx 3 \times 10^4$ $L_\odot$) deeply embedded in the W33 dense molecular cloud core ($A_V \approx$ 50–150 magnitudes; Capps et al. 1978). The large optical depths of the silicate and H_2O features towards W 33A show that it is a very young source (Capps et al. 1978; Soifer et al. 1979). Nevertheless, some OH maser emission is associated with this source, indicating that an HII region is already forming (Elitzur & de Jong 1978; Zheng 1994; Menten 1997). The detection of the Br α hydrogen recombination line confirms the presence of ionized hydrogen, although this is probably primarily associated with stellar winds rather than a standard HII region (Bunn et al. 1995). Furthermore, the rather small quantity of solid CO shows that warm-up and sublimation of the icy grain mantles has started (Smith et al. 1989; Tielens et al. 1991; Chiar et al. 1998). This places W 33A beyond the initial collapse phase (Helmich et al. 1999; Caselli et al. 1993).

3. Observations

The 7–8 μm spectra of W 33A and, for comparison, the high mass YSO NGC 7538 : IRS9 were obtained with ISO–SWS in the high resolution grating mode ($R = \lambda/\Delta\lambda \sim$1500). A selected region of these spectra was published in the CH_4 studies of Boogert et al. (1996; 1998). We re-reduced the spectra with version 6.0 of the SWS pipeline and the calibration files available in August 1998. The after-pipeline processing was similar to the method described in Boogert et al. (1998). However, since in this paper we focus on weak, broad dust features, special care was taken in the recognition of and correction for large scale dark current memory effects and detector response residuals. We averaged the 12 detector scans per scan direction, and found an excellent match between the 'up' and 'down' spectra for W 33A, indicating a proper dark current correction. However, for the brighter object NGC 7538 : IRS9 we find that the up spectrum has a 4% steeper slope between 7 and 8 μm. Given that the up spectrum was observed latest in time, with a more relaxed dark current, we corrected for this difference by tilting the down spectrum toward the up spectrum and then averaging the two. Local variations, i.e. on a scale of 0.1 μm, between the scans are negligible, except for a feature at 7.9 μm which appears in the up spectrum of NGC 7539 : IRS9 only, and thus its reality is uncertain. Finally, we checked our spectra for proper detector response correction by reducing an ISO–SWS spectrum of the the standard star α Lyrae with the same method as our observations. Except for high frequency instrumental fringing (see discussion in Boogert et al. 1998), no obvious correlations exist with spectral features seen in our spectra, and thus we conclude that the detector response correction in this wavelength region is reliable.

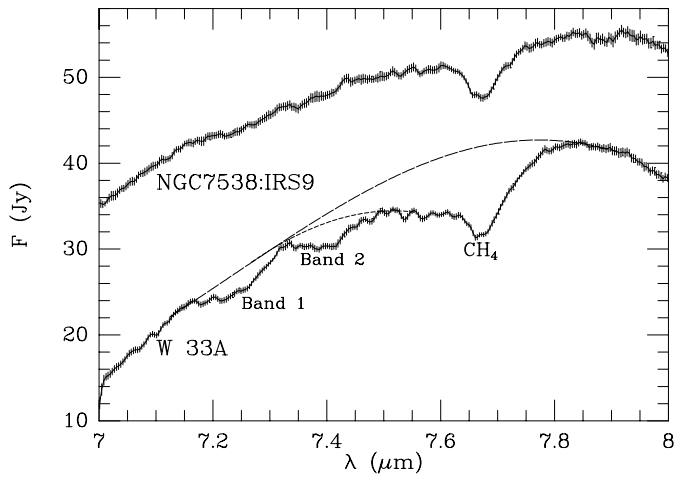

Fig. 1. The 7 to 8 μm SWS-AOT6 spectra towards W 33A and NGC7538:IRS9 (R = 850). Features are present at 7.24, 7.41, 7.63 (broad) and 7.67 μm (due to solid CH_4; Boogert et al. 1996). The long-dashed curve gives a 7th order polynomial baseline fit. The short-dashed curve indicates a 7th order polynomial used to extrapolate the broad 7.63 μm feature for separation from band 2.

At the radial velocity of W 33A (v_{LSR} = 33 km s^{-1}; Mitchell et al. 1990) the doppler shift is negligible (< 0.1 cm^{-1}/5 $\times$ 10^{-4} μm), and no correction was applied.

Fig. 1 shows the fully reduced spectra. The errorbars shown are not statistical, but instead have been derived from the difference between the up and the down scans. Most of the weak structure between 7.45–7.85 μm can be identified as ro-vibrational absorption lines of gaseous CH_4 (Boogert et al. 1998). A number of broad absorption features can be discerned. The strongest band at 7.67 μm has been previously identified with solid methane (Boogert et al. 1996). The underlying broader feature, centered at $\sim$ 7.63 μm, was tentatively assigned to solid SO_2 on the basis of low resolution ground based and airborne data (Boogert et al. 1997). This feature will be discussed in a future paper. In addition, two features are present at 7.24 and 7.41 μm for W 33A. Table 1 lists the spectral properties of these bands. (Integrated) Optical depths were obtained relative to the indicated baseline. In addition, the overlap between band 2 and

Table 1. Spectroscopic properties of band 1 and 2

		Band 1	Band 2
		W 33A	
Position	μm	7.243 ± 0.01	7.414 ± 0.01
	cm^{-1}	1381 ± 2	1349 ± 2
FWHM	μm	0.10 ± 0.02	0.08 ± 0.02
	cm^{-1}	19 ± 4	15 ± 3
τ^{a}_{int}	cm^{-1}	2.0 ± 0.3	1.6 ± 0.5
τ		0.10 ± 0.02	0.10 ± 0.03
		NGC7538:IRS9	
τ^{a}_{int}	cm^{-1}	≤ 0.5	≤ 0.3
τ		≤ 0.03	≤ 0.02

[a] Optical depth integrated over the feature.

the broad 7.63 μm feature was taken into account by using the extrapolation of the latter band as indicated in Fig. 1. Errorbars reflect statistical errors as well as the uncertainty introduced by the baseline selection and separation (band 2).

Earlier ground-based spectroscopy already showed indications of the 7.41 μm feature (Lacy et al. 1991). Some hint of the 7.24 μm feature may also be present in the NGC7538:IRS9 spectrum, but the S/N limitations prevent a definite identification in this case. The considerable widths of these bands and the absence of sharp structure of ro-vibrational transitions show that they originate in the solid state. We will denote the 7.24 and 7.41 μm features "Band 1" and "Band 2", respectively.

4. Comparison to the Galactic Center

A solid state infrared absorption feature towards a dense cloud source could have its origin either in condensed icy material or in the refractory grain cores. If coming from refractory material, the absorption could also be found in spectra of sources obscured by the diffuse medium. In particular, sources in the Galactic Center suffer considerable diffuse extinction (Tielens et al. 1996) and are therefore excellent probes of weak refractory dust features. Thus, in order to constrain their origin, we compare band 1 and 2 of W 33A with similar features towards the GC.

The spectrum of the galactic center, which probes dust in the diffuse medium, shows a weak absorption at 7.27 μm, close to 7.24 μm band of W 33A (Lutz et al. 1996; Chiar et al., in preparation). Moreover, the weakness of the 7.24 and 7.41 μm bands of W 33A may well preclude their detection towards the galactic center in view of the much smaller dust column density towards the latter source. Hence, an origin of these weak features in the refractory hydrocarbon dust component in the diffuse ISM cannot be entirely excluded.

5. Experimental procedure

The general procedure to create the ice samples and measure their infrared spectra has been described earlier (Hudgins et al. 1993; Gerakines et al. 1995). Compounds used in this work and their purities are as follows: formic acid (HCOOH; liquid), J. T. Baker, 98% purity; formamide ($\mathrm{HCONH_2}$; liquid), Merck, 99.5% purity; pentane ($\mathrm{C_5H_{12}}$; liquid), Baker, 99% purity; acetaldehyde ($\mathrm{CH_3HCO}$; liquid), Merck, 99% purity; methanol ($\mathrm{CH_3OH}$; liquid), Janssen Chimica, 99.9% purity; ammonia ($\mathrm{NH_3}$; gas), Indugas, 99.96% purity; hydrazine ($\mathrm{N_2H_4}$), purified aqueous solution (see Boudin et al. 1998).

To produce mixed ice samples suitable as astrophysical ice analogs we have the option to either pre-mix the constituent gases in a glass container, and deposit the mixed gas, or make two independent depositions, where the mixing only takes place on the 10 K substrate. In general, the first option was used. As an exception, formamide was deposited separately, since its low vapor pressure prevents production of a pre-mixed gas of accurate composition. Furthermore, the bases $\mathrm{NH_3}$ and $\mathrm{N_2H_4}$ and the acid HCOOH had to be deposited separately, because of reactivity.

Details on the properties of the UV lamp used to photolyze ice samples were described by Gerakines et al. (1996; and references therein). The lamp flux equals $\sim 1 \times 10^{15}$ photons $\mathrm{cm^{-2}\,s^{-1}}$ ($\mathrm{E}_{photon} > 6\,\mathrm{eV}$).

Table 2. Species considered for the 7.24 and 7.41 μm absorption bands. For details, see text.

Eliminated	alkenes, Toluene ($\mathrm{C_6H_5 - CH_3}$)
	Ethylbenzene ($\mathrm{C_6H_5 - CH_2CH_3}$), HOOCCOOH
	$\mathrm{CH_3COOH}$, $\mathrm{CH_3COCH_3}$, $\mathrm{CH_3CONH_2}$
Band 1	alkanes ($\mathrm{N_C} \geq 4$), $\mathrm{HCONH_2}$, HCOOH
Band 2	$\mathrm{CH_3HCO}$, $\mathrm{HCOO^-}$

6. Comparison to laboratory spectroscopy

Band 1 and 2 fall in the region characteristic for the CH deformation modes of organic species. This leaves numerous possible candidates. However, the focus should be on small molecules, since theory and observations indicate that grain chemistry favors the production of simple species over similar larger molecules (e.g., Boudin et al. 1998). Table 2 gives a listing of species which were surveyed. A first selection was made based on room temperature spectra found in standard infrared libraries (Aldrich, Sadtler). These usually correspond to pure liquids. The spectrum of the formate ion ($\mathrm{HCOO^-}$) was measured in a solution of $\mathrm{NH_3}$ and HCOOH in $\mathrm{H_2O}$ (Ito & Bernstein 1956). Liquid samples could be spectroscopically similar to amorphous ices in view of their disordered structure. A candidate was eliminated if its closest deformation mode is more than 0.05 μm (9 $\mathrm{cm^{-1}}$) away from either of the observed positions, or if the molecule has additional features which are clearly not present (i.e., in the current data or ground-based observations; e.g., Allamandola et al. 1992). This criterium is consistent with an "in retrospect" comparison of the spectra of the liquids and the various mixed amorphous ice samples containing the molecules selected for our experimental study (Sect. 6). For 4 of the 5 species the difference in position of the relevant features between these phases was $\leq 6\,\mathrm{cm^{-1}}$. On the other hand, for one of the molecules in our study (i.e., formic acid/HCOOH)

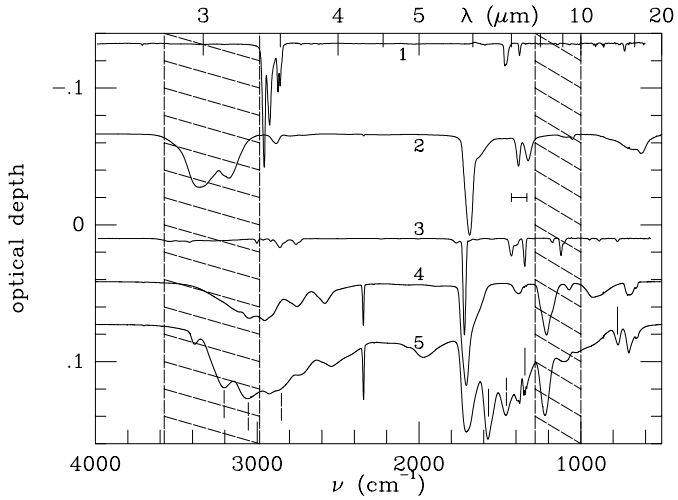

Fig. 2. Mid-Infrared spectra of the candidates selected for comparison to the band 1 and 2 of W 33A: 1. Pentane (C_5H_{12}); 2. Formamide ($HCONH_2$); 3. Acetaldehyde ($HCOCH_3$); 4. Formic acid (HCOOH); 5. The formate ion ($HCOO^-$). Except for $HCOO^-$, all spectra correspond to pure ices (apart from a minor CO_2 contamination apparent from the sharp feature at 2340 cm^{-1}). $HCOO^-$ was obtained in situ by warm-up to 80 K of the binary ice HCOOH/NH_3 = 1/0.4 (For details, see text). Solid vertical lines adjacent to spectrum 5 indicate features of $HCOO^-$, dashed lines indicate NH_4^+ bands. The horizontal bar marks the 7.0–7.5 μm region of special interest to this study. The shaded areas indicate the regions of the strong interstellar H_2O and silicate absorptions.

Table 3. Accessible infrared features of the candidate molecules.

Molecule	mode	Pos. cm^{-1}	Pos. μm	A cm
HCOOH	ν(C=O)	1710	5.85	6.7 (-17)[a]
	δ(CH)	1380	7.25	2.6 (-18)
$HCOO^-$	ν(C-O)	1580	6.33	1.0 (-16)[b]
	δ(CH)	1380	7.25	8.0 (-18)
	ν(C-O)	1350	7.41	1.7 (-17)
$HCONH_2$	ν(C=O)	1690	5.92	3.3 (-17)[c]
	δ(CH)	1385	7.22	3.2 (-18)
CH_3HCO	ν(C=O)	1715	5.83	1.3 (-17)[c]
	δ(CH)	1350	7.41	1.5 (-18)
C_5H_{12}	$\nu_{as}(-CH_3)$	2960	3.38	5.0 (-18)
	$\nu_{as}(-CH_2-)$	2930	3.41	4.8 (-18)
	$\nu_s(-CH_3)$	2875	3.48	1.5 (-18)
	$\nu_s(-CH_2-)$	2865	3.49	1.3 (-18)
	$\delta(-CH_2-)$/ $\delta_{as}(-CH_3)$	1460	6.85	1.2 (-18)
	$\delta_s(-CH_3)$	1380	7.25	3.3 (-19)[c]

[a] Maréchal 1987
[b] Appendix A
[c] Wexler 1967

the difference between liquid and amorphous ice was as large as 30 cm^{-1}. However, we feel that a substantial extension of our search parameters is not expedient before the candidates that are compliant with the present more restrictive choice have been thoroughly assessed by spectroscopy and comparison with the observations.

After the elimination process, we were left with 3 candidates for band 1, namely formic acid (HCOOH), formamide ($HCONH_2$), and alkanes ($\geq$ 4 C atoms; the $-CH_3$ deformation mode), and 2 candidates for band 2, namely acetaldehyde (CH_3HCO) and the formate ion ($HCOO^-$). Pentane (C_5H_{12}) was chosen to represent the alkanes. For alkanes with 4 or more C atoms, the CH vibrational modes vary very little between species. The smallest alkanes, methane and ethane, do not provide a good fit to band 1 (cf., Boogert et al. 1996; Boudin et al. 1998).

To provide a fundamental basis for comparison with the ISO data, Fig. 2 shows the full mid-infrared spectra of our candidates. Except for the formate ion, the spectra were all obtained for pure ices after deposition at 10 K. $HCOO^-$ was produced in situ by warm-up to 80 K of a mixture HCOOH/NH_3 = 10/4, leading to the formation of $HCOO^-$ and NH_4^+ through acid-base reactions (see Appendix A). The positions of the $HCOO^-$ and NH_4^+ features are indicated. As shown by Fig. 2, all species in this study have, apart from their CH deformation modes, other strong bands outside of the regions obscured by the interstellar silicate and H_2O absorptions that should be accessible by ISO. Table 3 lists these features. The positions are only approximate, since features can shift by typically $\sim 5\,cm^{-1}$ as a function of matrix composition and temperature. Except for $HCOO^-$, band strengths A were obtained from the literature for a selected feature. Other bands were than calibrated relative to this feature from the intensities measured in an H_2O ice matrix (H_2O/molec. $\approx$ 10/1). For $HCOO^-$ band strengths were obtained in an H_2O matrix from the balance between $HCOO^-$ formation and HCOOH disappearance during warm-up (Appendix A).

To enable a detailed comparison with the observed features, the candidate species were embedded in 2 different astrophysical ice analog matrices, namely H_2O ice (H_2O:cand. $\approx$ 10:1) and a mixture of H_2O and CH_3OH (H_2O:CH_3OH:can. $\approx$ 10:5:1). Separate H_2O-dominated and methanol-rich ice phases are indicated by detailed fitting of the spectral features towards high-mass YSO's (Skinner et al. 1992; Palumbo et al. 1995; Boogert et al. 1999; Gerakines et al. 1999; Ehrenfreund et al., in preparation). The abundance of CO in apolar ice, the third interstellar ice phase, equals 0.5–2.5% relative to H_2O for W 33A (Chiar et al. 1998). This is much lower than the CO abundances found towards sources of which the ices have experienced little thermal processing, e.g., Elias 16 and NGC7538:IRS9 (Chiar et al. 1998). This indicates that for W 33A the apolar ice mantles have evaporated along most of the line of sight (Tielens & Whittet 1997).

This study only considers a limited sample of ice matrices for spectroscopic comparison to the 7.24 and 7.41 μm bands. Indeed, rather than doing a full spectroscopic study for each of our candidates, we will focus on an initial verification of the plausibility of the selected species and to point out the opportunities to look for further diagnostic features. A full spectroscopic study

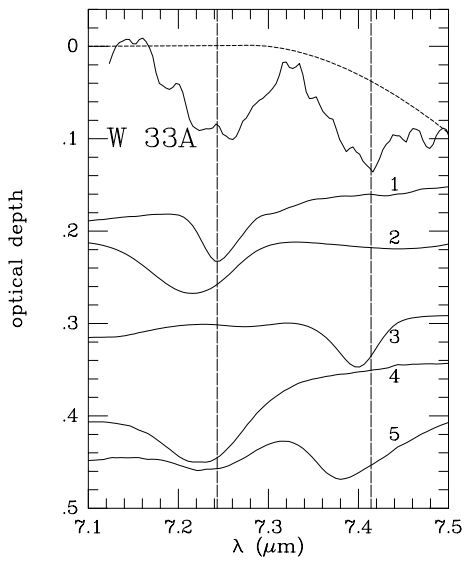

Fig. 3. Comparison between band 1 and 2 of W 33A and laboratory spectra of 1. Pentane (C_5H_{12}); 2. Formamide ($HCONH_2$); 3. Acetaldehyde ($HCOCH_3$); 4. Formic acid (HCOOH); 5. Formic acid and the Formate ion ($HCOO^-$). Except for no. 5, all spectra were obtained in H_2O-dominated ices (no CH_3OH) directly after deposition at 10 K (Tables 4 and 5). The $HCOO^-$ is embedded in $H_2O/HCOOH/NH_3/HCOO^-/NH_4^+$ = 100/3.2/3.2/0.4/0.4. The contribution by HCOOH was subtracted from this spectrum. (for details, see text). The optical depth plot was obtained by subtraction of the baseline (Fig. 1) from the original spectrum in the log(F) vs λ plane. Vertical lines trace the positions of the W 33A bands.

awaits the analysis of the entire mid-infrared spectrum, which should provide considerably more stringent constraints on the candidates, as well as a more firm basis for detailed spectroscopic comparison and selection of plausible ice matrices.

Tables 4 and 5 give the spectral characteristics of the various species as a function of temperature. The spectral properties were measured for the molecule inside analog matrices as well as for the pure ice. For $HCOO^-$ the simplest possible matrix that could be studied is a mixture of NH_3 and HCOOH.

The $HCOO^-$ ion was produced in situ by low temperature acid-base reactions involving formic acid (Appendix A). As a base we used NH_3 and in one case hydrazine (N_2H_4). The composition of the deposited gas mixtures, again reproducing the H_2O-dominated and CH_3OH-rich ice environments observed towards high-mass YSO's, is given by Table 5. Immediately after the deposition some $HCOO^-$ is already present. Since the conversion increases with temperature, the $HCOO^-$ concentration in these samples is variable (Appendix A).

In general, the spectral properties of the candidate features depend only weakly on matrix and temperature (Table 4 and 5). An exception is the ν(C-O) feature of the $HCOO^-$ ion near 1350 cm^{-1} (7.41 μm), which shifts up to 10 cm^{-1} between mixtures. On the other hand, this band does not shift very much when using N_2H_4 instead of NH_3 as proton acceptor.

$HCOO^-$ and HCOOH both produce a feature near 1380 cm^{-1} (7.25 μm). Thus, since $HCOO^-$ is produced by deposition and warm-up of HCOOH together with a base, these two components will blend as long as the conversion of formic acid to the formate ion is incomplete (i.e., for T $\lesssim$ 120 K; see Appendix A).

Fig. 3 compares the W 33A spectrum with the modes of the five candidates. The optical depth plot of W 33A was obtained by subtracting a 7th order polynomial baseline fit (Fig. 1) from the spectrum in the log(F) vs λ plane. We note here that this procedure does not represent a "true" continuum correction, which is hampered by the complexity of the spectrum in this region which comprises absorption by the red wing of the H_2O 6 μm band, the blue wing of the silicate band, and possibly aromatic absorption features as well, but should only be considered a "cosmetic" operation, enabling a better comparison with laboratory data. The extrapolation of the broad 7.63 μm band (Fig. 1) is also shown to better indicate the true extend of band 2. The laboratory spectra correspond to the H_2O-dominated matrices (H_2O:cand. $\approx$ 10/1; see Tables 4 and 5). $HCOO^-$ was measured in a matrix $H_2O/HCOOH/NH_3/HCOO^-/NH_4^+$ = 100/3.2/3.2/0.4/0.4, obtained after 10 K deposition of H_2O, HCOOH and NH_3 (Appendix A; Table 5). While in the original spectrum the HCOOH δ(CH) band dominates the 1380 cm^{-1} feature, in the curve as displayed in Fig. 1 this contribution has been taken out by appropriate subtraction of the spectrum of H_2O/HCOOH = 100/10. The residual structure at 1380 cm^{-1} can than be fully ascribed to the δ(CH) mode of $HCOO^-$.

It can be seen that the CH deformation mode of HCOOH lies close to band 1. Table 5 shows that HCOOH in a methanol-rich matrix also provides a fairly good match. On the other hand, the formamide δ(CH) feature lies blueward of band 1. This discrepancy holds for pure formamide as well as for formamide embedded in CH_3OH-rich ice, and is neither remedied at higher temperatures (Table 4). The pentane feature matches the position of band 1 quite well, especially at 10 K (Table 4), but is clearly too narrow. Again, this discrepancy does not change significantly with matrix (Table 4). However, if aliphatic hydrocarbons would be responsible for band 1, it seems likely that a mixture of such molecules is present along the line of sight. This could possibly result in the required broadening of the CH deformation feature.

Band 2 is reasonably well matched by $HCOO^-$ as well as CH_3HCO. The $HCOO^-$ feature is blue-shifted. However, inspection of Table 5 shows that this band is quite sensitive to the matrix composition. In view of the expected complexity of the interstellar matrix, this may give rise to the discrepancy. The CH_3HCO feature is slightly too narrow in the comparison shown by Fig. 3, however, the feature may perhaps broaden when more complex matrices are used.

We note that, due to the constraint set to the $HCOO^-$ abundance by the relatively small intensity of band 2, the contribution of the $HCOO^-$ feature near 1380 cm^{-1} (7.24 μm) to band 1 of W33 A is at most $\sim$ 35% (cf., Table 1 and Table 3). We will for the remainder ignore this possible contribution.

In summary, the comparison between the W 33A features and the spectra of our candidates still allows at least 2 possibilities for each of the observed bands. An assignment to formamide

Table 4. Positions and widths of the modes of the candidate species in various ice matrices. The features are seperated into those close to band 1 and those close to band 2.

Molecule	Matrix			T	Band 1		Band 2	
	H_2O	CH_3OH	cand.	K	pos. cm^{-1}	FWHM cm^{-1}	pos. cm^{-1}	FWHM cm^{-1}
C_5H_{12} pentane	100		10	10	1380.5	11.3		
				50	1379.4	12.4		
				80	1379.2	11.5		
				120	1379.5	10.9		
	100	40	20	10	1379.9	11.5		
				50	1378.2	11.3		
				80	1378.2	11.4		
				120	1377.8	11.6		
			pure	10	1379.5	11.0		
				50	1378.3	11.4		
				80	1372.9	9.3		
				120	1372.0	6.9		
$HCONH_2$ formamide	100		10	10	1385.5	23.0		
				50	1385.8	22.5		
				80	1386.0	22.2		
				120	1386.5	22.3		
	100	63	36	10	1386.9	20.2		
				50	1387.1	20.1		
				80	1387.6	19.9		
				120	1388.3	19.7		
			pure	10	1384.8	26.0		
				50	1384.6	25.5		
				80	1384.5	24.6		
				120	1384.9	24.0		
CH_3HCO acetaldehyde	100		15	10			1351.5	10.6
				50			1351.0	10.5
				80			1350.6	9.3
				120			1349.8	9.4
	100	36	14	10			1349.6	12.3
				50			1348.9	12.3
				80			1348.3	12.1
				120			1348.1	8.7
			pure	10			1346.0	14.6
				50			1345.8	14.5
				80			1346.0	13.9

appears less likely due to the discrepancy in position with the observed feature (band 1).

Table 6 provides the abundances of the candidate species implied if either band 1 or 2 is so assigned.

7. Other accessible infrared features

As seen from Fig. 2 and Table 2, all molecules in the present study show, besides the rather weak features close to band 1 or 2, other absorption bands of considerably higher intensity. Since the full mid-infrared spectrum of W 33A is being accessed by ISO, these features may soon be revealed. However, at the moderate to low abundance for the carriers implied by the intensity of the W 33A bands (Table 6), such features would have to lie outside the strong H_2O 3 μm band as well as the steep blue wing of the silicate 10 μm feature to be detectable.

Aliphatic hydrocarbons like pentane all have a strong 4-component feature around 3.4 μm (2900 cm^{-1}) due to the $-CH_3$ and $-CH_2-$ asymmetric and symmetric stretching modes. This region was already observed from the ground. (Allamandola et al. 1992). If band 1 originates in the $\delta(-CH_3)$ mode of saturated hydrocarbons, the corresponding asymmetric stretching mode should have $\tau_{int} \approx 30\,cm^{-1}$ (Tables 1 and 3). Position and width would be 2960 cm^{-1} (3.38 μm) and $\sim$ 20 cm^{-1} (0.02 μm; measured for the H_2O/pentane binary mixture; Table 4), implying $\tau \approx 1.6$. The observations by Allamandola et al. (1992) exclude the presence of such a strong feature. On the other hand, if the $-CH_3$ group is attached to an unsaturated chain, its deformation mode becomes $\sim$ 10 times stronger, while the intensity of the stretching feature decreases by 40% (Wexler 1967). Scaled to the intensity of band 1, this

Table 5. Positions and widths of the modes of the candidate species close to band 1 and 2 (cont.).

Molecule	Matrix					T	Band 1		Band 2	
	H_2O	CH_3OH	NH_3	N_2H_4	cand.	K	pos. cm^{-1}	FWHM cm^{-1}	pos. cm^{-1}	FWHM cm^{-1}
HCOOH formic acid	100				10	10	1382.8	26.5		
						50	1382.6	24.7		
						80	1383.1	25.7		
						120	1380.7	18.1		
	100	40			12	10	1380.0	16.7		
						50	1380.8	15.3		
						80	1381.9	16.4		
					pure	10	1385	42		
						50	1381	42		
						80	1378	52		
						120	1376	43		
$HCOO^-$ formate ion	100		3.6		3.6[a]	10	1382.3[b]	19.8	1354.4	17.8
						50	1382.3[b]	19.1	1354.4	19.2
						80	1382.2[b]	18.8	1353.6	19.8
						120	1383.9[b]	17.4	1349.8	20.0
	100	41	10		10[a]	10	1381.9[b]	19.2	1353.5	20.1
						50	1383.7[b]	20.0	1354.3	19.6
						80	1383.5[b]	19.7	1355.2	18.8
						120	1383.8[b]	17.8	1356.4	17.3
	100			2.7	10[a]	10	1381.5[b]	19.9	1354.6	18.2
						50	1380.8[b]	20.2	1354.6	16.8
						80	1380.4[b]	18.5	1354.6	16.4
						120	1381.5[b]	17.1	1353.8	15.4
			4		10[a]	10	1380.4[b]	38	1346.9	26
						50	1379.0[b]	34	1345.5	34
						80	1379.0[b]	28	1345.1	31

[a] Refers to the deposited abundance of HCOOH.
[b] Feature is a blend of bands of $HCOO^-$ and HCOOH, the $HCOO^-$ contribution increasing with increasing temperature (Table 3; Appendix A).

would bring the CH stretching mode below the present detection limit (i.e., $\tau \lesssim 0.1$). Also, the required abundance of the carrier would be 10 times less (cf., Table 6). However, under these conditions the $\delta_{as}(-CH_3)$ mode shifts redward by about 10 cm^{-1} (0.05 μm; Wexler 1967) and would not provide a good match to band 1 anymore. We conclude that, while not fully excluded, the deformation mode of aliphatic $-CH_3$ groups seems an unlikely assignment for band 1.

Fig. 2 and Table 3 show that, with the exception of pentane, the strongest accessible features of our candidates lie in the 1800–1400 cm^{-1} (5.55–7.15 μm) region. The C=O stretching modes of formic acid, formamide and acetaldehyde all produce strong features near 1700 cm^{-1} (5.9 μm; Table 3, Fig. 2). For aldehydes the feature is sharper than for organic acids and amides. $HCOO^-$ produces a very strong C-O stretching mode at 1580 cm^{-1} (6.33 μm), while pentane gives a feature at 1460 cm^{-1} (6.85 μm), caused by combined deformation modes of $-CH_2-$ and $-CH_3$.

To predict how all these features may show up in the ISO spectra, we constructed the spectra for the mixtures H_2O:X at the ratio indicated by the strengths of band 1 and 2 (Table 6). This construction is based on the spectra obtained in the H_2O-dominated matrices (Tables 4 and 5), to which the spectrum of pure amorphous H_2O ice was mathematically added to the extent required to arrive at the correct ratio. The spectrum including $HCOO^-$ was based on the 10 K ice mixture $H_2O/HCOOH/NH_3/HCOO^-/NH_4^+$ = 100/3.2/3.2/0.4/0.4 (Table 5, Appendix A), with, again, H_2O added to obtain the $HCOO^-$ abundance suggested by the observations (Table 6).

Table 6. Abundances towards W33 A implied by an assignment of band 1 or 2 to the various candidate species

Molecule	A (cm molec.$^{-1}$)		Abundances	
	Band 1	Band 2	vs H_2O[a]	vs H[b]
HCOOH	2.6(-18)		2.6(-2)	2.7(-6)
$HCOO^-$		1.7(-17)	3.1(-3)	3.4(-7)
$HCONH_2$	3.2(-18)		2.1(-2)	2.2(-6)
CH_3HCO		1.5(-18)	3.6(-2)	3.8(-6)
C_5H_{12}	3.3(-19)		2.0(-1)	2.2(-5)

[a] Assuming N(H_2O ice) = 3.0×10^{19} cm^{-2}, as determined from the 6 μm feature (Keane et al., in preparation).
[b] Using N(H) = 2.8×10^{23} cm^{-2} (Tielens et al. 1991).

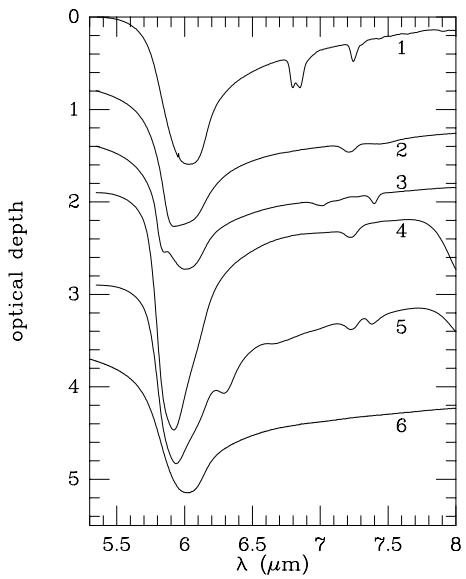

Fig. 4. 5–8 micron spectra corresponding to the candidates diluted in H_2O ice at 10 K. 1. Pentane (C_5H_{12}); 2. Formamide ($HCONH_2$); 3. Acetaldehyde ($HCOCH_3$); 4. Formic acid (HCOOH); 5. The formate ion ($HCOO^-$). The spectra correspond to the same ice mixtures used for Fig. 3. However, the spectrum of pure H_2O was in each case mathematically added in order to arrive at the H_2O/X ratio expected for W 33A. (Table 6). Spectrum 6 corresponds to pure H_2O (10 K). All spectra correspond to an H_2O column density of 3.0×10^{19} molec. $cm^{-2}\,s^{-1}$. Arbitrary offsets have been applied. For details, see text.

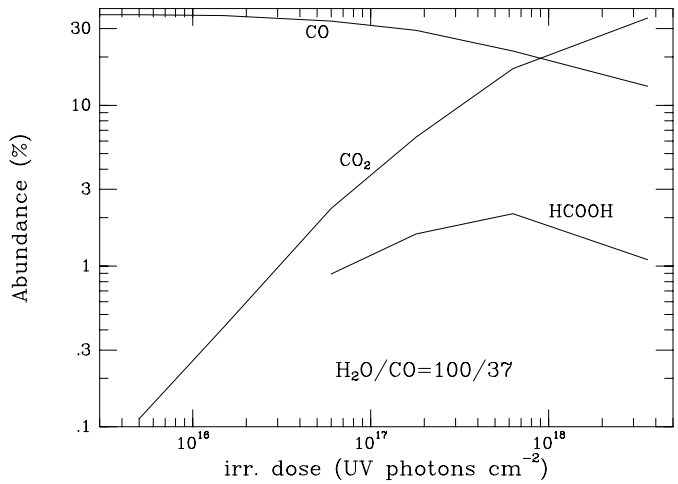

Fig. 5. The abundances of CO, CO_2 and HCOOH relative to the original deposited quantity of H_2O as a function of irradiation dose for the sample H_2O/CO=100/37

The results are shown in Fig. 4. All spectra correspond to an H_2O column density of $3.0 \times 10^{19}\,cm^{-2}$. It can be seen that the broad ν(C=O) features of HCOOH and $HCONH_2$ become fully blended with the 6 μm H_2O band, causing a distinct blueshift of this feature. The shift is strongest with HCOOH, as its ν(C=O) feature lies further to the blue (Table 3). In addition, the blending causes a clear enhancement of the 6 μm feature, especially with the strong HCOOH band. For $HCOO^-$ and CH_3HCO clear characteristic spectral structure is present on top of the 6 μm feature, corresponding to their ν(C-O) and ν(C=O) modes, respectively (Table 3). With pentane, the CH deformation mode at 1460 cm^{-1} (6.85 μm) shows up alongside the 1380 cm^{-1} (7.24 μm) band. However, it seems likely that this feature, if present, would become fully blended with the strong unidentified 6.8 μm absorption feature which is generally observed towards high mass YSO's (Schutte et al. 1996; Tielens & Allamandola 1987; Keane et al., in preparation).

HCOOH was previously proposed as a constituent of the icy mantles towards NGC7538:IRS9 (Schutte et al. 1996). Its presence was inferred from a red excess absorption on the observed 6 μm feature, which is reproduced if the H_2O 6 μm band is blended with the C=O stretching mode of an organic acid (cf., Fig. 4). The corresponding column density was $2.4 \times 10^{17}\,cm^{-2}$, i.e., $\sim$ 3% of that of solid H_2O. In comparison, the upper limit to the intensity of band 1 towards NGC7539:IRS9 (Table 1) indicates N(HCOOH) $\leq 1.9 \times 10^{17}\,cm^{-2}$. This slight discrepancy may indicate that other species, e.g., higher organic acids, contribute part of the red excess, although higher S/N observations and a definite detection of the 7.21 μm band are required to verify this possibility. Nevertheless, the observations indicate similar HCOOH abundances relative to H_2O for NGC7538:IRS9 and W 33A (Table 6). This suggests that HCOOH may be a general constituent of the ices near high mass YSO's.

We conclude that verification of the presence of the present candidates for band 1 and 2 of W 33A should become possible once the entire 5–8 μm spectrum has been analyzed (Keane et al., in preparation). However, we note that evidence is accumulating that HCOOH is present in interstellar ices.

8. Discussion

The strength of the band 1 and 2 would typically correspond to abundances of a few percent for the carrier (Table 6). This can be compared to results of theoretical or experimental simulation of the chemistry of interstellar grains. The formation of formic acid, formamide and acetaldehyde on grain surfaces is initiated by the reaction of CO with H. The resulting radical HCO can react with atomic O, N and C to ultimately lead to HCOOH, $HCONH_2$ and CH_3HCO. Theoretical grain surface chemistry calculations predict abundances of the order of 1% for the former two for a wide range of conditions (Tielens & Hagen 1982). In these models, the calculated acetaldehyde production was very low because of the low abundance of gaseous atomic C. Currently, observations indicate much higher atomic C abundances in molecular clouds, perhaps reflecting the presence of cosmic ray produced FUV photons inside dense clouds (cf., Schilke et al. 1995), and hence grain surface chemistry may lead to considerably higher acetaldehyde abundances than previously anticipated.

As an alternative, HCOOH may also be produced photochemically (Greenberg et al. 1980; Hagen 1982). Information on UV-photolyzed laboratory ices is available from the Leiden database (http://www.strw.leidenuniv.nl/~lab; see also Ger-

akines et al. 1996). As a representative example, Fig. 5 shows the photochemical evolution of the ice mixture H_2O/CO=100/37. The major photoproduct is CO_2, with minor products being HCOOH, as well as H_2CO, HCO, and CH_3OH (not shown in Fig. 5; cf., d'Hendecourt et al. 1986). The photoproduction was traced by monitoring the δ(OH) band of HCOOH near $1220\,\mathrm{cm}^{-1}$ (Fig. 2), and the CO_2 ν_3 band near $2340\,\mathrm{cm}^{-1}$. Band strengths of these features were adapted from Gerakines et al. 1995 and Maréchal 1987. The maximum HCOOH abundance of 2.1% of H_2O is attained after an exposure of $\sim 6 \times 10^{17}$ photons cm^{-2}. Such an exposure is well within the plausible dose range that may be collected by a grain inside a dense cloud (Whittet et al. 1998). The maximum abundance is close to the quantity corresponding to band 1 of W 33A (Table 6). However, while the initial quantity of CO in this sample may be consistent with theoretical predictions of the composition of ices condensing under general dense cloud conditions (depending on the efficiency adopted for the conversion of CO by grain surface chemistry; cf., d'Hendecourt et al. 1985; Grim & d'Hendecourt 1986; Tielens & Whittet 1997; Hiraoka et al. 1994; 1998; Schutte 1998), it far exceeds the actually observed abundance of CO embedded in H_2O ice (e.g., Tielens et al. 1991; Chiar et al. 1998). In view of the high abundance of CO_2 in interstellar ices (de Graauw et al. 1996b; Whittet et al. 1998), perhaps this discrepancy is partially explained by the conversion of CO to CO_2 during the irradiation. Another possibility is that the CO in the initial condensation is gradually depleted by selective desorption (Schutte & Greenberg 1991; Hasegawa & Herbst 1993). Other factors that could influence the efficiency of photochemical HCOOH production are the spectrum of the incident UV radiation, or the presence of other carbon bearing molecules besides CO in the initial condensation, e.g., CO_2 (e.g., Tielens & Whittet 1997).

9. Conclusions

SWS spectroscopy towards the heavily obscured young stellar object W 33A reveals absorption features at 7.24 and 7.41 μm. Their width, and the absence of ro-vibrational fine structure, indicates a solid-state origin. Comparison to laboratory spectra of a number of molecules embedded in H_2O ice shows that close correspondence can be found with the CH deformation mode of HCOOH for the 7.24 μm feature and with either the CH deformation mode of CH_3HCO or the CO stretching mode of $HCOO^-$ for the 7.41 μm feature. Somewhat less likely is an assignment of the 7.24 μm band to the aliphatic $-CH_3$ deformation mode, due to the absence of complementary structure in the CH stretching region near 3.4 μm. $HCONH_2$ should not yet be excluded, but its CH deformation mode seems to be consistently too far to the blue. In the near future, verification of these possibilities by ISO observations of additional features, especially in the 5.5–7 μm region, should be straightforward.

The abundance of the species implied by the intensity of the observed absorption features considerably exceeds the predictions of models of dense cloud gas and grain surface chemistry. This indicates that the main production pathways for these species may yet have to be discovered. These could either involve alternative grain surface reactions, or energetic processing. If the assignment of the 7.41 μm feature to $HCOO^-$ is correct, its production does not need energetic processing if HCOOH can, in one way or another, be produced by grain surface chemistry.

After NGC7538:IRS9, W 33A is the second massive YSO for which the presence of solid formic acid at the abundance level of a few percent is implied by the observations. This may indicate that this molecule is a general constituent of ices near such objects.

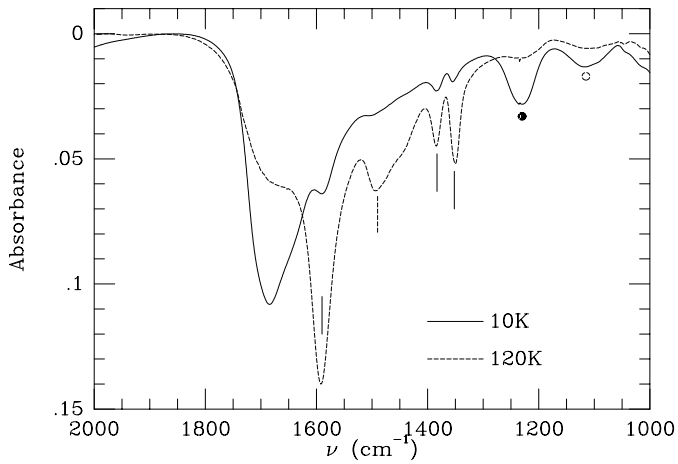

Fig. A1. Spectral evolution of the mixture H_2O/HCOOH/NH_3 = 100/3.6/3.6 as a function of temperature. Solid lines indicate features due to $HCOO^-$, dashed line NH_4^+, filled dot HCOOH, open dot NH_3.

Acknowledgements. Special thanks go to Richard Ruiterkamp and Nathalie Boudin for their assistance in the experimental and data processing effort. Comments by the referee, Bernard Schmitt, greatly improved the clarity of this paper. This work was partially funded by NASA grant NGR 33-018-148 and by an ASTRON grant from the Netherlands Organization for Scientific Research (NWO). Support for W.S. from SRON is acknowledged as well. D.C.B.W. is funded by NASA grants NAGW-3144 and NAGW-4039. J.E.C. holds a National Research Council-ARC Research Associateship.

Appendix A: production of $HCOO^-$

It is well known that in many cases acid-base reactions can proceed in the solid phase at cryogenic temperatures (Ritzhaupt & Devlin 1977; Zundel & Fritsch 1984; Grim & Greenberg 1987; Grim et al. 1989; Schutte & Greenberg 1997; Demyk et al. 1998). By the same token, in-situ production of $HCOO^-$ was achieved by depositing HCOOH together with a base (either N_2H_4 or NH_3) inside an astrophysically relevant ice matrix. Fig. A1 shows the spectral evolution of the ice deposition H_2O/HCOOH/NH_3 = 100/3.6/3.6 during warm-up. It can be seen that, when the temperature is raised to 120 K, the features of HCOOH and NH_3 decrease, while bands grow at 1384, 1350, 1592 and $1490\,\mathrm{cm}^{-1}$, as well as 3205, 3050, 2950 and $770\,\mathrm{cm}^{-1}$ (See also Fig. 2). This suggests that proton exchange occurs and new charged species are formed. Comparison to

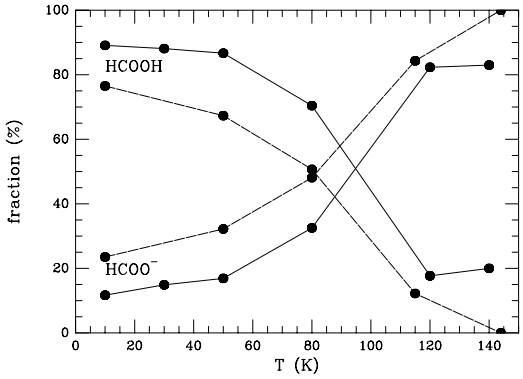

Fig. A2. Conversion HCOOH to $HCOO^-$ during warm-up. The y-axis gives, as a function of temperature, the fraction of the originally deposited quantity of HCOOH converted to $HCOO^-$ or remaining as HCOOH. Solid line corresponds to the deposition H_2O/NH_3/HCOOH = 100/3.6/3.6, dashed line to H_2O/CH_3OH/HCOOH/NH_3 = 100/41/10/10.

spectra of $HCOO^-$ and NH_4^+ in cryogenic matrices, aqueous solutions at room temperature, or in salt pellets (Ritzhaupt & Devlin 1977; Demyk et al. 1998; Ito & Bernstein 1956) leads to an assignment of the 1384, 1350, 1592 and 770 cm^{-1} features to $HCOO^-$, while the 1490, 3205, 3050, and 2950 cm^{-1} are due to NH_4^+. These assignments were verified by exchanging either the acid or the base, with iso-cyanic acid or hydrazine, respectively (Boudin et al. 1998, Keane & Schutte, in preparation).

Band strengths for $HCOO^-$ (Table 3) were obtained straightforwardly from the balance of $HCOO^-$ formation and HCOOH disappearance during warm-up in the H_2O/NH_3/HCOOH = 100/3.6/3.6 experiment. The amount of $HCOO^-$ produced during warm-up to 120 K is simply equal to the amount of HCOOH that is converted, which can be obtained from the decrease of the ν(C=O) feature of HCOOH (Table 3). This information, together with the growth of the $HCOO^-$ features upon warm-up, yields the band strengths. Due to the close correspondence of the δ(CH) features of HCOOH and $HCOO^-$ (Table 3), the contribution of each molecule in the 10 and 120 K spectra to the 1380 cm^{-1} feature was assessed from other bands, i.e., the ν(C=O) feature of HCOOH and the ν(C-O) feature of $HCOO^-$. To do this, we used the 120 K spectrum to obtain the relative intensities of the $HCOO^-$ bands, since at this temperature the contribution of HCOOH to the 1380 cm^{-1} feature is negligible (Fig. 6). In this way the increase of the $HCOO^-$ δ(CH) band could be correctly calibrated.

Fig. A2 shows the conversion of HCOOH to $HCOO^-$ as a function of temperature for H_2O/HCOOH/NH_3 = 100/3.6/3.6 and H_2O/CH_3OH/HCOOH/NH_3 = 100/41/10/10. It can be seen that the conversion continuously increases with temperature. The conversion is slightly larger in the methanol containing mixture, probably caused by the larger concentration of the acid and base in the ice matrix. Some ions are already present directly after the deposition at 10 K. This can be ascribed to reactions between acids and bases in neighboring sites, possibly aided by the heat of condensation. The small increase of the ion abundance during warm-up to 30 K shows that the activation barrier of the acid-base reaction is negligible, and that the rate of conversion vs. T is determined by barriers against diffusion keeping HCOOH and NH_3 apart, rather than reaction barriers.

References

Allamandola L.J., Sandford S.A., Tielens A.G.G.M., Herbst T.M., 1992, ApJ 399, 134

Boogert A.C.A., Schutte W.A., Tielens A.G.G.M., et al., 1996, A&A 315, L377

Boogert A.C.A., Schutte W.A., Helmich F.P, Tielens A.G.G.M., Wooden D.H., 1997, A&A 317, 929

Boogert A.C.A., Helmich F.P, van Dishoeck E.F., et al., 1998, A&A, in press

Boogert A.C.A., Ehrenfreund P., Gerakines P.A., et al., 1999, submitted to A&A

Boudin N., Schutte W.A., Greenberg J.M., 1998, A&A 331, 749

Bunn J.C., Hoare M.G., Drew J.E., 1995, MNRAS 272, 346

Capps R.W., Gillett F.C., Knacke R.F., 1978, ApJ 226, 863

Caselli P., Hasegawa T.I., Herbst E., 1993, ApJ 408, 548

Charnley S.B., Tielens A.G.G.M., Millar T.J., 1992, ApJ 399, L71

Chiar J.E., Gerakines P.A., Whittet D.C.B., et al., 1998, ApJ 498, 716

Demyk K., Dartois E., d'Hendecourt L., et al., 1998, A&A, in press

d'Hendecourt L.B., Allamandola L.J., Greenberg J.M., 1985, A&A 152, 130

d'Hendecourt L.B., Allamandola L.J., Grim R.J.A., Greenberg J.M., 1986, A&A 158, 119

de Graauw Th., Haser L.N., Beintema D.A., et al., 1996a, A&A 315, L49

de Graauw Th., Whittet D.C.B., Gerakines P.A., et al., 1996b, A&A 315, L345

Elitzur M., de Jong T., 1978, A&A 67, 323

Geballe T.R., Baas F., Greenberg J.M., Schutte W., 1985, A&A 146, L6

Gerakines P.A., Schutte W.A., Greenberg J.M., van Dishoeck E.F., 1995, A&A 296, 810

Gerakines P.A., Schutte W.A., Ehrenfreund P., 1996, A&A 312, 289

Gerakines P.A., Whittet D.C.B., Ehrenfreund P., et al., 1999, submitted to ApJ

Greenberg J.M., Allamandola L.J., Hagen W., van de Bult C.E.P., Baas F., 1980, In: Andrew B.H. (ed.) Interstellar Molecules. Proc. IAU symp. 87, Kluwer, Dordrecht, p. 355

Grim R.J.A., d'Hendecourt L.J., 1986, A&A 167, 161

Grim R.J.A., Greenberg J.M., 1987, ApJ 321, L91

Grim R.J.A., Greenberg J.M., de Groot M.S., et al., 1989, A&AS 78, 161

Grim R.J.A., Baas F., Geballe T.R., Greenberg J.M., Schutte W., 1991, A&A 243, 473

Hagen W., 1982, Ph.D. Thesis, University of Leiden, The Netherlands

Hasegawa T.I., Herbst E., 1993, MNRAS 261, 83

Helmich F.P., Millar T.J., van Dishoeck E.F., 1999, submitted to A&A

Hiraoka K., Ohashi N., Kihara Y., et al., 1994, Chem. Phys. Letters 229, 408

Hiraoka K., Miyagoshi T., Takayama T., Yamamoto K., Kihara Y., 1998, ApJ 498, 710

Hudgins D.M., Sandford S.A., Allamandola L.J., Tielens A.G.G.M., 1993, ApJ 86, 713

Ito K., Bernstein H.J., 1956, Can. J. Chem. 34, 170

Kessler M.F., Steinz J.A., Anderegg M.E., et al., 1996, A&A 315, L27

Lacy J.H., Baas F., Allamandola L.J., et al., 1984, ApJ 276, 533

Lacy J.H., Carr J.S., Evans II N.J., et al., 1991, ApJ 376, 556
Lutz D., Feuchtgruber H., Genzel R., et al., 1996, A&A 315, L269
Maréchal Y., 1987, J. Chem. Phys. 87, 6344
Menten K.M., 1997, In: van Dishoeck E.F. (ed.) Molecules in Astrophysics: Probes and Processes. Proc. IAU symp. 178, Kluwer, Dordrecht, p. 163
Mitchell G.F., Maillard J.-P., Allen M., Beer R., Belcourt K., 1990, ApJ 363, 554
Palumbo M.E., Tielens A.G.G.M., Tokunaga A.T., 1995, ApJ 449, 674
Ritzhaupt G., Devlin J.P., 1977, J. Phys. Chem. 81, 521
Schilke P., Keene J., Le Bourlot J., Pineau de Forêts G., Roueff E., 1995, A&A 294, L17
Schutte W.A., 1998, In: Ehrenfreund P., Kochan H., Krafft C., Pirronello V. (eds.) Laboratory Astrophysics and Space Research. Kluwer, Dordrecht, in press
Schutte W.A., Greenberg J.M., 1991, A&A 244, 190
Schutte W.A., Greenberg J.M., 1997, A&A 317, L43
Schutte, W.A., Tielens, A.G.G.M., Whittet, D.C.B., et al., 1996, A&A 315, L333
Schutte W.A., Greenberg J.M., van Dishoeck E.F., et al., 1998, Ap&SS 255, 61
Schutte W.A., Greenberg J.M., van Dishoeck E.F., et al., 1998a, in: Waters L.B.F.M., Waelkens C., van der Hucht K.A., Zaal P. (eds.) ISO's view on stellar evolution, Kluwer, Dordrecht, p. 61
Skinner C.J., Tielens A.G.G.M., Barlow, M.J., Justtanont K., 1992, ApJ 399, L79
Smith R.G., Sellgren K., Tokunaga A.T., 1989, ApJ 344, 413
Soifer B.T., Puetter R.C., Russell R.W., et al., 1979, ApJ 232, L53
Tielens A., 1989, In: Allamandola L.J., Tielens A.G.G.M Interstellar Dust. Proc. IAU symp. 135, Kluwer, Dordrecht, p. 239
Tielens A.G.G.M., Allamandola L.J., 1987, In: Morfill G.E., Scholer M. (eds.) Physical Processes in Interstellar Clouds. p. 333
Tielens A.G.G.M., Hagen W., 1982, A&A 114, 245
Tielens A.G.G.M., Whittet D.C.B., 1997, In: van Dishoeck E.F. (ed.) Molecules in Astrophysics: Probes and Processes. Proc. IAU symp. 178, Kluwer, Dordrecht, p. 45
Tielens A.G.G.M., Tokunaga A.T., Geballe T.R., Baas F., 1991, ApJ 381, 181
Tielens A.G.G.M., Wooden D.H., Allamandola L.J., Bregman J., Witteborn F.C., 1996, ApJ 461, 210
Wexler A.S., 1967, Applied Spectr. Rev. 1, 29
Whittet D.C.B., Schutte W.A., Tielens A.G.G.M., et al., 1996, A&A 315, L357
Whittet D.C.B., Gerakines P.A., Tielens A.G.G.M., et al., 1998, ApJ 498, L159
Zheng X., 1994, Chin. Astron. Astrophys. 18, 443
Zundel G., Fritsch J., 1984, J. Phys Chem 88, 6295